

Conductance and Kondo Interference Beyond Proportional Coupling

Luis G. G. V. Dias da Silva,¹ Caio H. Lewenkopf,² Edson Vernek,³ Gerson J. Ferreira,³ and Sergio E. Ulloa⁴

¹*Instituto de Física, Universidade de São Paulo, C.P. 66318, 05315-970 São Paulo, SP, Brazil*

²*Instituto de Física, Universidade Federal Fluminense, 24210-346 Niterói, Brazil*

³*Instituto de Física, Universidade Federal de Uberlândia, Uberlândia, Minas Gerais 38400-902, Brazil.*

⁴*Department of Physics and Astronomy, and Nanoscale and Quantum Phenomena Institute, Ohio University, Athens, Ohio 45701-2979, USA*

(Dated: February 28, 2017)

The transport properties of nanostructured systems are deeply affected by the geometry of the effective connections to metallic leads. In this work we derive a conductance expression for interacting systems whose connectivity geometries do not meet the Meir-Wingreen proportional coupling condition. As an interesting application, we consider a quantum dot connected coherently to tunable electronic cavity modes. The structure is shown to exhibit a well-defined Kondo effect over a wide range of coupling strengths between the two subsystems. In agreement with recent experimental results, the calculated conductance curves exhibit strong modulations and asymmetric behavior as different cavity modes are swept through the Fermi level. These conductance modulations occur, however, while maintaining robust Kondo singlet correlations of the dot with the electronic reservoir, a direct consequence of the lopsided nature of the device.

PACS numbers: 73.63.Kv, 72.10.Fk, 72.15.Qm

The quantum coupling of spatially localized discrete levels to cavity modes has emerged as a key tool for quantum information processing in different contexts, from cavity systems in atoms [1] and semiconductor quantum dots [2] to exciton-polariton condensates in optical systems [3]. Similarly, coherent coupling of electronic modes to discrete quantum systems has been explored in quantum corrals created on metallic surfaces [4], allowing the manipulation and control of quantum information over regions a few nanometers across [5]. Recent experiments have extended this fascinating line of inquiry to systems implemented on two-dimensional electronic structures in semiconductors [6, 7]. These new systems have paved the way for quantum engineering in integrated, scalable nanoscale systems with great flexibility on geometries and interesting physical behavior.

The control of quantum dot (QD) characteristics in these systems, such as the tunnel coupling to external current leads, have also allowed the experimental study of the Kondo regime, an emblematic many-body effect [8, 9]. In this regime, the net magnetic moment of an unpaired spin in the QD becomes effectively screened by the conduction electrons in the leads, forming a delocalized quantum singlet that involves correlations with the electronic spins in the lead reservoirs [10]. Moreover, the coupling of a QD to reservoirs with non-trivial energy dependence gives rise to a variety of interesting effects on the ensuing Kondo state, including the appearance of zero-field splittings of the Kondo resonance [11–13]. As QD systems are designed to interact with increasingly complex structures, one is led to ask how such many-body correlations would evolve.

The standard theoretical tool for the description of the two-terminal conductance through interacting regions is the Meir-Wingreen (MW) generalization of the Landauer formula for correlated systems [14]. The MW expression

is particularly useful in cases where the coupling matrix elements between the leads and the system are related to each other by a multiplicative factor. This condition was later dubbed “proportional coupling” (PC) [15] and it is essential in writing the conductance in terms of the system’s retarded Green’s function. In many cases, however, the PC description is inadequate [16] and the evaluation of the conductance requires an alternative treatment.

A remarkable example of a nanoscale device with non-PC geometry was recently investigated at the ETH [6]. They demonstrated coherent coupling between a QD in the Coulomb blockade regime and a larger, cavity-like region inscribed electrostatically onto the same two-dimensional electron gas (2DEG). The QD is coupled to two metallic leads while the cavity itself is coupled to only one of them, clearly breaking the PC condition. The size of the cavity and its coupling to the QD can be controlled by gate voltages on the device, allowing for fine control over the spacing between cavity resonances, the tunnel rate of electrons between cavity and QD, and the dot-cavity coupling over a wide range, while studying the conductance of the entire structure.

In this paper we generalize and extend the MW expression for the conductance to non-PC cases, providing theoretical tools to analyze systems with complex structures, as some studied recently [6, 7]. We find it is possible to write the linear conductance of the system as

$$G = \frac{2e^2}{h} \frac{\Gamma_L(\varepsilon_F)\Gamma_R(\varepsilon_F)}{\Gamma_L(\varepsilon_F) + \Gamma_R(\varepsilon_F)} \int d\omega \left(-\frac{\partial f_0}{\partial \omega} \right) A_d(\omega), \quad (1)$$

where f_0 is the equilibrium Fermi function, the couplings $\Gamma_{L,R}(\varepsilon_F)$ are effective hybridization functions to left (L) and right (R) leads, $A_d(\omega) = (-1/\pi)\text{Im} G_d^r(\omega)$ the spectral function, and G_d^r is the retarded Green’s function at the QD. The latter two functions can be accurately calculated through a variety of techniques, such as Wil-

son's numerical renormalization group (NRG) [17]. Although deceptively similar to the MW conductance formula, this expression incorporates the connection to each lead through the hybridization functions $\Gamma_{L,R}(\varepsilon_F)$ and their intricate energy structure. As we will see below, these functions can be obtained after careful consideration of the effective connectivity of the system.

Next, we use this approach to successfully describe and provide further insight on conductance measurements of a QD coupled to a cavity [6]. We implement a realistic model of the curved electrostatic reflector used to define the cavity in experiments, utilizing both analytical and numerical approaches. We further calculate the QD spectral density required by Eq. (1) by applying NRG to an effective Anderson model that incorporates the cavity. Our results show contrasting transport properties in the weak- and strong-coupling regimes, in excellent agreement with experiments. As the coupling to the cavity sets in, the conductance is strongly modulated, especially as different cavity resonances are swept through the Fermi level in the leads by applied gates [6]. Moreover, the NRG calculations allow us to relate the conductance behavior to other intrinsic characteristics, such as the Kondo temperature T_K . We find that even as the conductance peaks are strongly distorted due to the interaction with the cavity modes, the Kondo screening remains robust, with larger T_K values for stronger cavity coupling.

MW formula beyond proportional coupling. Proportionally coupled systems are those in which the decay widths of the interacting system to L and R leads are proportional to each other, namely, $\Gamma_R(\omega) = \lambda \Gamma_L(\omega)$, where λ is a constant factor [14]. This condition is clearly violated in the case of a QD connected to a cavity on only one lead, such as in Fig. 1. An electron in the dot is transmitted to L by a direct tunneling process regulated by the coupling matrix element V_{dL} and the density of states in that lead. In contrast, the transmission to the right involves the coherent interference between multiple paths that include the cavity resonances and states in R . Figure 1(b) indicates the different dot-cavity (Ω), dot-lead (V_{dR}), and cavity-lead (V_{cR}) couplings that contribute to the interference and energy dependence of $\Gamma_R(\omega)$, making the decay widths evidently non-proportional.

The main technical difficulty in obtaining a transport formula for non-proportionally coupled systems is the elimination of the lesser Green's function $G^<$ for the interacting region (the QD here), which appears in the general expression for the current [14]. The current through the QD through either L or R leads is

$$J_{L(R)} = \frac{ie}{h} \int d\omega \Gamma_{L(R)}(\omega) \left\{ G^<(\omega) + f_{L(R)}(\omega) [G^r(\omega) - G^a(\omega)] \right\}, \quad (2)$$

where $G^{r(a)}$ is the retarded (advanced) Green's function and $f_{L(R)}$ is the Fermi distribution in each lead with chemical potential $\mu_{L(R)}$. For non-PC systems away from equilibrium, $G^<$ elimination is not straightforward. It

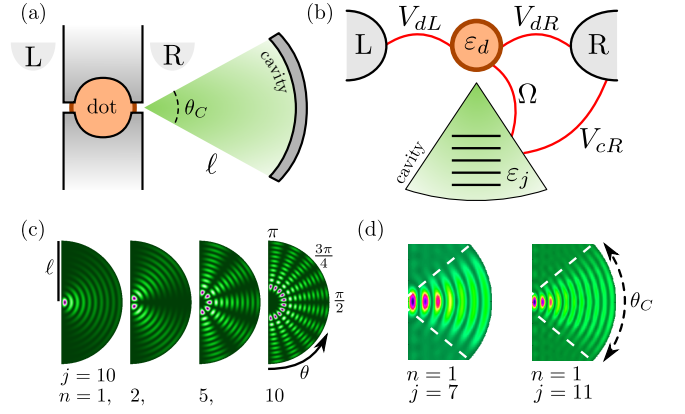


FIG. 1. (a) Experimental dot+cavity system; the cavity has radius ℓ and aperture θ_C . (b) Schematic of single-level dot (ε_d) coupled to multi-mode cavity (ε_j). The dot is connected to leads (L and R), while cavity is only coupled to the R -lead; coupling matrix elements are indicated. (c) Cavity modes for $\theta_C = \pi$ are described by Bessel modes $\psi_{n,j}(r, \theta)$. The $n = 1$ modes dominate the LDOS at $r \approx 0$. (d) Kwant mode simulation for finite aperture cavity ($\theta_C = \pi/2$) coupled to wide leads shows good agreement with Bessel modes.

can, however, be achieved by using a key approximation in linear response: that $G^<$ and $\partial G^</\partial \mu$ are slowly-varying functions of ω within a window $k_B T$ [16], so that

$$G^<(\omega) = G_{\text{eq}}^<(\omega) + \frac{\partial G^<}{\partial \mu} \Delta \mu + O(\Delta \mu^2), \quad (3)$$

and $\partial G^</\partial \mu \simeq (-\partial f_0 / \partial \omega) \Pi(\omega)$, where $\Pi(\omega)$ has a smooth ω dependence and $\Delta \mu = \mu_L - \mu_R$. These conditions eventually lead to Eq. (1); the detailed derivation is provided in the supplement [18]. Notice that the structure of the system may result in a cumbersome derivation of the decay widths $\Gamma_{L,R}$ entering Eq. (1). We now specify the QD-cavity model that exemplifies this treatment.

Resonant cavity modes. The key experimental element is a “mirror” that focuses resonant modes onto the QD, both elements electrostatically defined on a 2DEG. The cavity has a length $\ell \sim 2 \mu\text{m}$ and angular aperture $\theta_C \sim 45^\circ$, as indicated in Fig. 1(a). Assuming circular symmetry, the normal modes are given by Bessel functions, $\psi_{n,j}(r, \theta) \simeq J_n(k_{n,j}r) \sin(n\theta)$. The dot-cavity coupling is maximal for modes with largest amplitude in the vicinity of $r \approx 0$, and dominated by resonances with $n = 1$, given that $J_n(kr) \propto (kr)^n$ for $kr \ll 1$. These modes have a characteristic energy spacing $\delta_{\text{cav}} \approx 200 \mu\text{eV}$ for a cavity with these dimensions, in agreement with the resonance separations in the experiment [6] and confirmed by Kwant calculations [18, 19].

It is remarkable that although the cavity is immersed in the R -lead, it can be tuned to produce sharply peaked resonances that strongly modify $\Gamma_R(\omega)$, providing different electronic paths for the current. In the experiment, a gate voltage shifts the cavity resonance levels and the coupling to the QD. This tunability can be incorporated in the interacting QD model as follows.

Interacting quantum impurity model. The Hamiltonian for this system can be written as $H = H_{\text{dot}} + H_{\text{cavity}} + H_{\text{leads}} + H_{\text{coupling}}$, where

$$H_{\text{dot}} = \sum_{\sigma} \varepsilon_d c_{d\sigma}^{\dagger} c_{d\sigma} + U n_{d\uparrow} n_{d\downarrow}, \quad (4)$$

$$H_{\text{cavity}} = \sum_{j,\sigma} \varepsilon_j a_{j\sigma}^{\dagger} a_{j\sigma}, \quad (5)$$

$$H_{\text{leads}} = \sum_{\alpha,\mathbf{k},\sigma} \varepsilon_{\alpha\mathbf{k}} c_{\alpha\mathbf{k}\sigma}^{\dagger} c_{\alpha\mathbf{k}\sigma}. \quad (6)$$

Here $c_{d\sigma}^{\dagger}$, $a_{j\sigma}^{\dagger}$, and $c_{\alpha\mathbf{k}\sigma}^{\dagger}$ create a spin- σ electron in the dot, the j th mode of the cavity, and each of the leads $\alpha = L, R$. The resonances are assumed equally spaced, $\varepsilon_j = \varepsilon_c + (j-1)\delta_{\text{cav}}$, where ε_c is shifted by a gate voltage; leads have a flat density of states $\rho(\omega) = \rho_0 \Theta(D - |\omega|)$, symmetric about the Fermi energy ($\omega = 0$). For simplicity all couplings are assumed local, real and independent of either momentum in the leads or cavity-mode index j . The coupling Hamiltonian is then, see Fig. 1(b),

$$H_{\text{coupling}} = \sum_{\alpha,\mathbf{k},\sigma} V_{d\alpha} c_{d\sigma}^{\dagger} c_{\alpha\mathbf{k}\sigma} + V_{cR} \sum_{j,\mathbf{k},\sigma} a_{j\sigma}^{\dagger} c_{R\mathbf{k}\sigma} + \Omega \sum_{j,\sigma} c_{d\sigma}^{\dagger} a_{j\sigma} + \text{H.c.} \quad (7)$$

QD effective decay widths. As the Coulomb interactions are localized in the QD, one can find its effective couplings to L and R leads and the cavity, by calculating the dot retarded Green's function for the system with $U = 0$, $G_d^{(0),r}(\omega^+) \equiv \langle\langle c_{d\sigma}; c_{d\sigma}^{\dagger} \rangle\rangle_{\omega}$. In the wide-band limit for the leads, $\sum_{\mathbf{k}} (\omega^+ - \varepsilon_{\mathbf{k}})^{-1} \rightarrow -i\pi\rho_0$, we obtain $G_d^{(0),r}(\omega) = (\omega - \varepsilon_d - \Sigma_d^{(0)}(\omega))^{-1}$, where

$$\Sigma_d^{(0)}(\omega) = -\frac{i}{2}(\Gamma_{dL} + \Gamma_{dR}) + \left(\Omega - \frac{i}{2}\sqrt{\Gamma_{dR}\Gamma_{cR}} \right)^2 \tilde{S}(\omega), \quad (8)$$

is the non-interacting self-energy. Here, $\Gamma_{(c,d)\alpha} \equiv 2\pi\rho_0|V_{(c,d)\alpha}|^2$, for $\alpha = L, R$, with the cavity structure contained in $S(\omega) \equiv \sum_j (\omega - \varepsilon_j)^{-1}$ and $\tilde{S}(\omega) = S(\omega)(1 + iS(\omega)\Gamma_{cR}/2)^{-1}$. The hybridization function of the (non-interacting) dot with the effective fermionic system is given by $\Delta(\omega) = -\text{Im}\Sigma_d^{(0)}(\omega)$. This approach can be extended to the interacting Green's function [12, 13], as long as the interactions are restricted to the QD.

The interference of cavity modes and states in the leads is contained in the structure of $\Delta(\omega)$, which yields a highly structured density of states of the “effective” Fermi reservoir in which the QD is embedded [18]. Most importantly, the structure in $\Delta(\omega)$ affects strongly the Kondo state in the system once interactions set in. $\Delta(\omega)$ reliably describes the experimental system once cavity parameters are extracted either from a microscopic model, and/or determined from experiments [20].

Conductance for the interacting system. Eq. (1) determines the conductance through the system under different cavity+QD coupling regimes. The QD coupling to

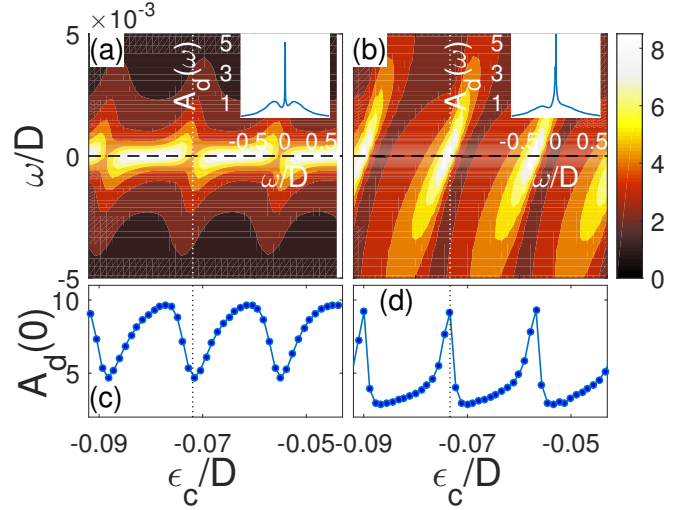


FIG. 2. NRG-calculated dot spectral density $A_d(\omega)$ for cavity gate voltages ε_c in the weak [$\Omega = 0.001D$, (a), (c)] and strong coupling [$\Omega = 0.025D$, (b), (d)] regimes. Panels (c) and (d) show $A_d(0)$ vs ε_c (cuts through the horizontal dashed lines). Peaks in $A_d(0)$ correspond to dips in $\Delta(0)$ and vice versa [18]. Insets show typical Kondo peaks in $A_d(\omega)$, present even when cavity modes dominate $\Delta(0)$ (vertical dotted lines).

the left (source) reservoir is simply $\Gamma_L = \Gamma_{dL}$. In contrast, the coupling to the right (drain) reservoir requires the full Green's function and results in [18]

$$\Gamma_R(\omega) = \Gamma_{dR} + \Gamma_{cR} |\tilde{S}(\omega)|^2 \left(\Omega^2 + \frac{\Gamma_{cR}\Gamma_{dR}}{4} \right) + \sqrt{\Gamma_{dR}\Gamma_{cR}} \tilde{S}(\omega) \left(\Omega - \frac{i}{2}\sqrt{\Gamma_{cR}\Gamma_{dR}} \right) + \text{H.c.} \quad (9)$$

This expression encodes information about all non-trivial interference processes taking place during transport. The energy dependence of $\Gamma_R(\omega)$ prevents the use of the PC simplification, demanding the more general approach we put forward here. The spectral function needed in Eq. (1) is obtained by an NRG approach that uses the full intricate structure of the effective hybridization function $\Delta(\omega)$ coupling the interacting QD to the environment.

Before discussing the conductance, we analyze the QD spectral function. In general, $A_d(\omega)$ shows a sequence of asymmetric features whenever ε_c shifts cavity modes near the Fermi level ($\omega = 0$), with characteristic shape and width that changes strongly with coupling Ω . Figure 2 illustrates this behavior for weak ($\Omega < \Gamma_{cR}/2$) and strong ($\Omega > \Gamma_{cR}/2$) dot-cavity coupling regimes. For weak coupling [Fig. 2(a)&(c)], the modulation is marked by diagonal “valleys” whenever a cavity mode contributes to $\Delta(0)$, separated by bright peaks in A_d . The large Ω regime [Fig. 2(b)&(d)] is drastically different: $\Delta(0)$ exhibits Fano asymmetric lineshapes as a function of ε_c , leading to sharp asymmetric peaks in $A_d(\omega < T_K)$ [18].

This behavior can be qualitatively understood in terms of the Friedel sum rule (FSR) [12, 21, 22], as $A_d(0)$ is

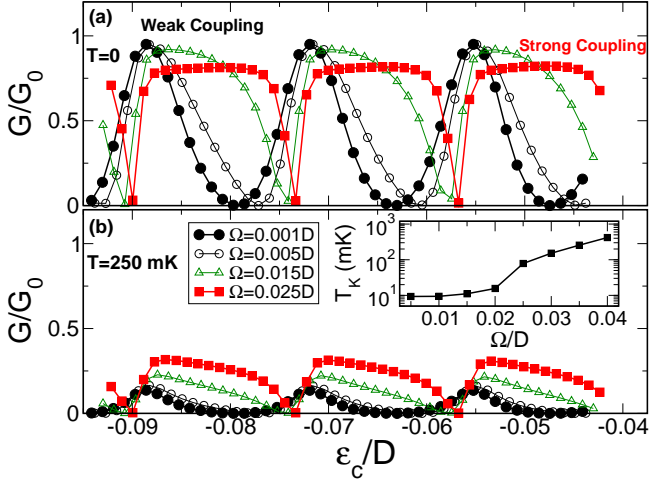


FIG. 3. Conductance G/G_0 for cavity gate voltages ϵ_c ranging from the weak ($\Omega = 0.001D$) to the strong coupling regime ($\Omega = 0.025D$) for (a) $T = 0$ and (b) $T = 0.031U$ (or $T = 250$ mK for $U = 0.7$ meV). Inset: Kondo temperature as a function of cavity-dot coupling Ω for $\epsilon_c = -0.09D$.

inversely proportional to $\Delta(0)$. Accordingly, when a resonant peak of $\Delta(\omega)$ lies close to the Fermi energy, it causes a downturn in the spectral function, and a consequent *splitting* of the Kondo peak may appear in A_d in the $\omega < T_K$ range [12]. Such splittings do appear for some ϵ_c values, where A_d shows two local maxima away from the $\omega = 0$ mark in Figs. 2(a) and (b) (see details in [18]). Nonetheless, even at these points, $A_d(\omega)$ shows fully-developed Kondo resonances of width $\sim T_K$ in between Hubbard peaks (insets in Figs. 2(a) and (b)).

The resulting conductance G (in units of $G_0 = 2e^2/h$) is shown in Fig. 3 vs cavity voltage ϵ_c , for Ω values from $0.001D$ (weak) to $0.025D$ (strong coupling) and for $T = 0$ & 250 mK. At low temperatures and small Ω , the conductance exhibits a quantized peak whenever a cavity resonance is near the Fermi level. The conductance drops away with ϵ_c as destructive interference sets in and results in a non-zero scattering shift associated with the strongly asymmetric $A_d(\omega)$, as expected from the FSR. Conversely, when a cavity resonance is aligned with the Fermi level in the strong coupling regime, a *dip* appears in the conductance, with otherwise sizeable value between resonances. Finite temperatures do not result in qualitative changes of this picture, but suppress the magnitude of G , as one would expect, with a larger effect for T_K values below the temperature of the reservoir (here 250 mK).

Notice that the spinful QD remains in the Kondo regime over this range of coupling to the cavity. In fact, the Kondo screening is stronger for larger Ω , as monitored by the value of T_K . To quantify this, we calcu-

late T_K from the magnetic susceptibility curves obtained from NRG, a procedure that focuses on how the Kondo fixed point is reached at lower energies, and does not rely on the behavior of the spectral density [17]. The inset in Fig. 3 shows T_K increasing rapidly with larger QD-cavity coupling Ω , with T_K reaching 400 mK in the strong coupling regime ($\Omega \gtrsim 0.02D$). For $\Omega = 0.025D$, we obtain $T_K \sim 0.0097U$; with the experimental $U = 0.7$ meV, this translates into $T_K \sim 80$ mK, in agreement with the observed value of ~ 100 mK, obtained from the conductance peak width (see supplement in [6]). Our calculations also show T_K to depend weakly on ϵ_c . This might appear counterintuitive, as $\Delta(0)$ is strongly modulated by changes in ϵ_c , but the explanation is simple: The effective coupling defining the Kondo temperature (e.g., Γ in Haldane's expression [23]) is given not by $\Delta(0)$, but rather by an integral over the full bandwidth, $\Gamma \propto \int \Delta(\omega) d(\omega/D)$ [24]. This “ Γ ” depends strongly on the dot-cavity coupling Ω (thereby giving the strong variation of T_K with Ω) while only weakly with ϵ_c , whose main effect is to shift the peaks in $\Delta(\omega)$.

The increasing T_K indicates that the screening of the QD spin by the composite cavity-lead environment is in fact more robust for larger Ω , which is confirmed by an NRG analysis of the thermal properties of the QD. This is remarkable behavior, as the strong variation in $A_d(\omega)$ and resulting conductance are drastically different from the simply-connected QD in the Kondo regime.

Discussion. We have presented an approach that allows one to calculate the conductance for strongly interacting systems beyond the proportional coupling approximation. This opens the possibility of studying interesting systems with complex geometries where quantum interference introduces non-trivial energy dependence on the effective decay widths Γ_α . We have illustrated the power of the method by analyzing a recent experiment with very interesting geometry [6]. Despite the observed splitting and strong modulation of conductance peaks for growing cavity coupling, we find that the Kondo screening is in fact strengthened, as characterized by a larger T_K . This interpretation is supported by calculations of the conductance in excellent agreement with experiment. It would be interesting to be able to measure the expected phase shifts introduced by the interaction with the cavity to provide further insights into the coherent interference that these many-body coupled systems experience.

We acknowledge useful discussions with C. Rössler, T. Ihn, K. Ensslin, and N. Sandler. LDS acknowledges support from CNPq grants 307107/2013-2 and 449148/2014-9, PRP-USP NAP-QNano and FAPESP grant 2016/18495-4. SEU received support from NSF grant DMR 1508325, and the Aspen Center for Physics, NSF grant PHY-1066293. CHL is supported by CNPq grant 308801/2015-6 and FAPERJ grant E-26/202.917/2015. GJF and EV acknowledge financial support from CNPq and FAPEMIG.

-
- [1] J. M. Raimond, M. Brune, and S. Haroche, *Rev. Mod. Phys.* **73**, 565 (2001).
 - [2] K. Hennessy, A. Badolato, M. Winger, D. Gerace, M. Atature, S. Gulde, S. Falt, E. L. Hu, and A. Imamoglu, *Nature* **445**, 896 (2007).
 - [3] J. Kasprzak, M. Richard, S. Kundermann, A. Baas, P. Jeambrun, J. M. J. Keeling, F. M. Marchetti, M. H. Szymanska, R. Andre, J. L. Staehli, V. Savona, P. B. Littlewood, B. Deveaud, and L. S. Dang, *Nature* **443**, 409 (2006).
 - [4] E. J. Heller, M. F. Crommie, C. P. Lutz, and D. M. Eigler, *Nature* **369**, 464 (1994).
 - [5] H. C. Manoharan, C. P. Lutz, and D. M. Eigler, *Nature* **403**, 512 (2000).
 - [6] C. Rössler, D. Oehri, O. Zilberberg, G. Blatter, M. Karalic, J. Pijnenburg, A. Hofmann, T. Ihn, K. Ensslin, C. Reichl, and W. Wegscheider, *Phys. Rev. Lett.* **115**, 166603 (2015).
 - [7] B. Brun, F. Martins, S. Faniel, B. Hackens, A. Cavanna, C. Ulysse, A. Ouerghi, U. Gennser, D. Mailly, P. Simon, S. Huant, V. Bayot, M. Sanquer, and H. Sellier, *Phys. Rev. Lett.* **116**, 136801 (2016).
 - [8] D. Goldhaber-Gordon, H. Shtrikman, D. Mahalu, D. Abusch-Magder, U. Meirav, and M. A. Kastner, *Nature* **391**, 156 (1998).
 - [9] S. M. Cronenwett, T. H. Oosterkamp, and L. P. Kouwenhoven, *Science* **281**, 540 (1998).
 - [10] A. C. Hewson, *The Kondo Problem to Heavy Fermions* (University Press, Cambridge, England, 1997).
 - [11] W. B. Thimm, J. Kroha, and J. von Delft, *Phys. Rev. Lett.* **82**, 2143 (1999).
 - [12] L. G. G. V. Dias da Silva, N. P. Sandler, K. Ingersent, and S. E. Ulloa, *Phys. Rev. Lett.* **97**, 096603 (2006).
 - [13] L. G. G. V. Dias da Silva, K. Ingersent, N. Sandler, and S. Ulloa, *Phys. Rev. B* **78**, 153304 (2008).
 - [14] Y. Meir and N. S. Wingreen, *Phys. Rev. Lett.* **68**, 2512 (1992).
 - [15] Y. Meir, N. S. Wingreen, and P. A. Lee, *Phys. Rev. Lett.* **70**, 2601 (1993).
 - [16] Y. Komijani, R. Yoshii, and I. Affleck, *Phys. Rev. B* **88**, 245104 (2013).
 - [17] R. Bulla, T. A. Costi, and T. Pruschke, *Rev. Mod. Phys.* **80**, 395 (2008).
 - [18] Find additional details in the supplementary document at XXX..
 - [19] C. W. Groth, M. Wimmer, A. R. Akhmerov, and X. Waintal, *New J. Phys.* **16**, 063065 (2014).
 - [20] The ETH structure [6] has charging energy $U = 700 \mu\text{eV}$; dot-source (left) and dot-drain (right) couplings $\Gamma_{dL} \approx \Gamma_{dR} \approx 87 \mu\text{eV}$; cavity broadening $\Gamma_{cR} \approx 40 \mu\text{eV}$; and cavity mode spacing $\delta_{cav} \approx 220 \mu\text{eV}$. Using $U = 0.5D \approx 700 \mu\text{eV}$, the NRG scales are then set as $\Gamma_{dL} = \Gamma_{dR} = 0.125U$, $\Gamma_{cR} = 0.06U$ and $\delta_{cav} = 0.32U$.
 - [21] L. Vaugier, A. A. Aligia, and A. M. Lobos, *Phys. Rev. B* **76**, 165112 (2007).
 - [22] L. G. G. V. Dias da Silva, E. Vernek, K. Ingersent, N. Sandler, and S. E. Ulloa, *Phys. Rev. B* **87**, 205313 (2013).
 - [23] F. D. M. Haldane, *Phys. Rev. Lett.* **40**, 416 (1978).
 - [24] C. Gonzalez-Buxton and K. Ingersent, *Phys. Rev. B* **57**, 14254 (1998).
-

Supplemental Material for *Conductance and Kondo Interference Beyond Proportional Coupling*

I. SYSTEM GEOMETRY AND MODEL PARAMETERS

The model parameters we use in this paper have been inferred from the experimental data from Ref. S6 combined with analytical estimates and numerical calculations. Here, we provide more details on the numerical simulations.

The experimental setup of Ref. S6 consists of a cavity focusing resonant modes into a quantum dot, both set on a GaAs two-dimensional electron gas (2DEG). The cavity has a radius $\ell \sim 2 \mu\text{m}$ and an angular aperture $\theta_C \sim 45^\circ$, as indicated in Fig. 1(a). To obtain a simple, yet accurate description of the non-interacting modes of the cavity, we consider its eigenstates to be approximately given by Bessel functions. The Bessel approximation becomes exact for a large aperture $\theta_C \rightarrow 180^\circ$, as the cavity approaches a semi-circle shape [Fig. 1(b)]. In the following we show that this approximation leads to a level spacing that agrees remarkably well with the experimental [S1] peak energy splitting $\delta_{cav} = 200 \mu\text{eV}$.

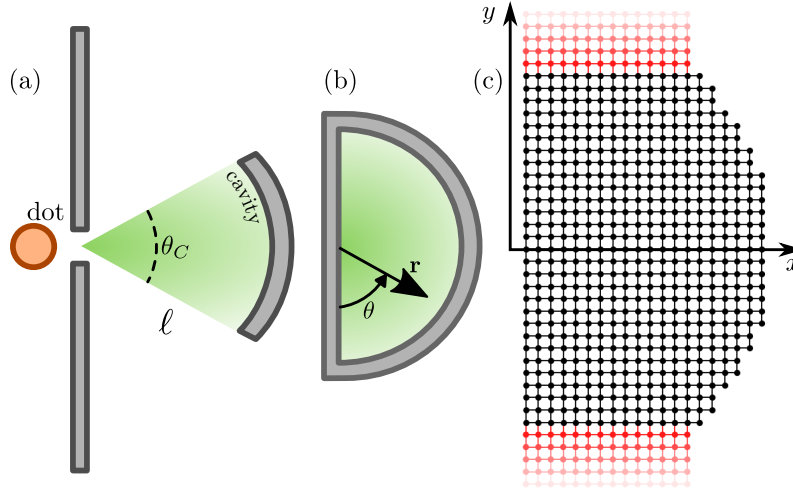


FIG. S1. (a) Illustration of the dot-cavity coupled system indicating the radius $\ell = 2 \mu\text{m}$ and angular aperture θ_C of the resonant cavity. (b) Two-dimensional system of coordinates $\mathbf{r} = (r, \theta)$ for the semi-circle approximation for the cavity modes corresponding to the limit $\theta_C \rightarrow 180^\circ$. (c) Example of the finite differences lattice model with leads (in red) implemented in Kwant. In this illustration the grid step size is large ($\sim 100 \text{ nm}$) for better visualization, while for the simulations the step size reduced ($\sim 2 \text{ nm}$).

Assuming hard-wall boundary conditions, the solution for the Schrödinger equation in cylindrical coordinates results in eigenstates $\psi_{n,j}(r, \theta)$ given by Bessel functions $J_n(z)$, and eigenenergies $\varepsilon_{n,j}$ set by the j^{th} zero $z_{n,j}$ of $J_n(z)$ at $r = \ell$, which reads

$$\psi_{n,j}(r, \theta) = C_{n,j} \sqrt{\frac{2}{\pi}} \sin(n\theta) J_n(k_{n,j}r), \quad (\text{S1})$$

$$\varepsilon_{n,j} = \frac{\hbar^2}{2m} \left(\frac{z_{n,j}}{\ell} \right)^2, \quad (\text{S2})$$

where $k_{n,j} = \sqrt{2m\varepsilon_{n,j}/\hbar^2}$, and $C_{n,j}$ is a normalization constant. To satisfy the boundary condition at the linear wall of the semi-circle ($x = 0$), the index $n = 1, 2, 3, 4, \dots$ must be a non-zero integer.

Near the Fermi level $k_{n,j} \approx k_F = 2\pi/\lambda_F$, where λ_F is the Fermi wavelength of the 2DEG under the resonant cavity. For $\ell \approx 2 \mu\text{m}$ one gets $k_{n,j}\ell \approx 2\pi\ell/\lambda_F \gg 1$, which allow us to use the asymptotic limit of the Bessel functions[S2] to find analytical expression for the zeros $z_{n,j}$. Since $J_n(z) \approx \sqrt{2/\pi z} \cos(z - n\pi/2 - \pi/4)$ we find

$$z_{n,j} = \frac{3\pi}{4} + \frac{\pi}{2}(n + 2j) = \frac{3\pi}{4} + \frac{\pi}{2}l \equiv z_l. \quad (\text{S3})$$

The n and j quantum labels become degenerate, and the Bessel zeros become simply z_l , with $l = (n + 2j)$. The integer

l is odd (even) whenever n is odd (even). Consequently $\varepsilon_{n,j} \rightarrow \varepsilon_l$ near the Fermi level,

$$\varepsilon_l = \frac{\hbar^2}{2m\ell^2} \left(\frac{3\pi}{4} + \frac{\pi}{2}l \right)^2. \quad (\text{S4})$$

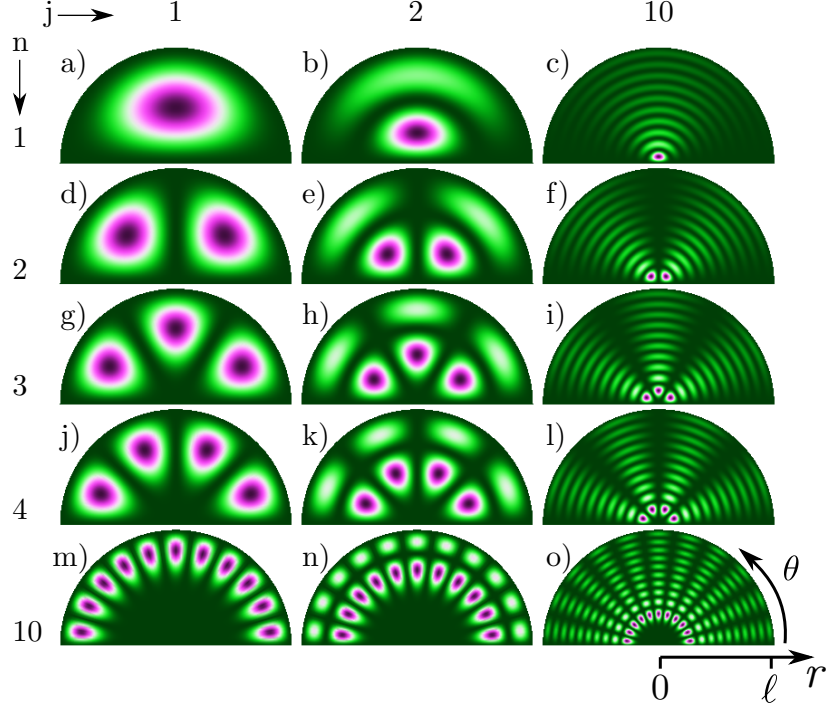


FIG. S2. Bessel modes $|\psi_{n,j}(r, \theta)|^2 \propto [\sin(n\theta)J_n(k_{n,j}r)]^2$ (see Eq. (S1)) representing the LDOS peaks of the resonant cavity of $\ell = 2 \mu\text{m}$. The panel lines correspond to $n = 1, 2, 3, 4$, and 10 , and the columns are for $j = 1, 2$, and 10 , as indicated. Excluding the boundaries, the number of nodes along θ is $n - 1$, and along r it is $j - 1$. The $n = 1$ modes dominates the LDOS near $r = 0$, where the cavity effectively couples to the dot.

The coupling of the dot with the resonant modes of the cavity occurs via the split-gate set by the linear electrodes in Fig. 1(a). Therefore the relevant quantity is the LDOS $\propto |\psi_{n,j}(r, \theta)|^2$ of the cavity modes in the vicinity of this region, i.e. $\mathbf{r} \sim 0$. Figure S2 shows $|\psi_{n,j}(r, \theta)|^2$ for different n and j . Since $J_n(kr) \propto (kr)^n$ for $kr \ll 1$, near $r = 0$ the dominant coupling must be given by $n = 1$, yielding odd l .

We conclude that the energy spacing between cavity resonant modes that are effectively coupled to the dot is

$$\delta_{cav} = \varepsilon_{l+2} - \varepsilon_l = \frac{\hbar^2}{2m\ell^2} \frac{\pi^2}{2} (5 + 2l). \quad (\text{S5})$$

Considering the experimental data of Ref. S6, $\lambda_F = 53 \text{ nm}$ and $\ell = 2 \mu\text{m}$, we obtain $\varepsilon_F \approx 8 \text{ meV}$ and $l \sim 150$ for $\varepsilon_l \sim \varepsilon_F$, corresponding to 75 even l and 75 odd l occupied resonant modes. From these we find $\delta_{cav} \approx 200 \mu\text{eV}$, which matches the experimental energy splitting between resonances reported in Ref. S6.

We compare the Bessel function approximation with a numerically calculated LDOS implemented using the Kwant code [S3]. Figure S3 shows a remarkably good agreement for both low energies and energies close the ε_F , corresponding to panels (a) and (b). Note that the even l states (blue dots) do not contribute to the LDOS near $r = 0$ as expected from the discussion based on Bessel eigenmodes. Panels (c)-(f) show the full LDOS map on the cavity for small energies, also in good agreement with the Bessel solutions shown in Fig. S2.

II. GREEN'S FUNCTIONS AND EQUATIONS OF MOTION

Our approach combines the equations-of-motion (EOM) with the numerical renormalization group (NRG) method to find the linear response current in strongly interacting systems. The EOM method allows us to assess the “single-particle” interference processes for arbitrarily complicated geometries and cast them in terms of effective energy

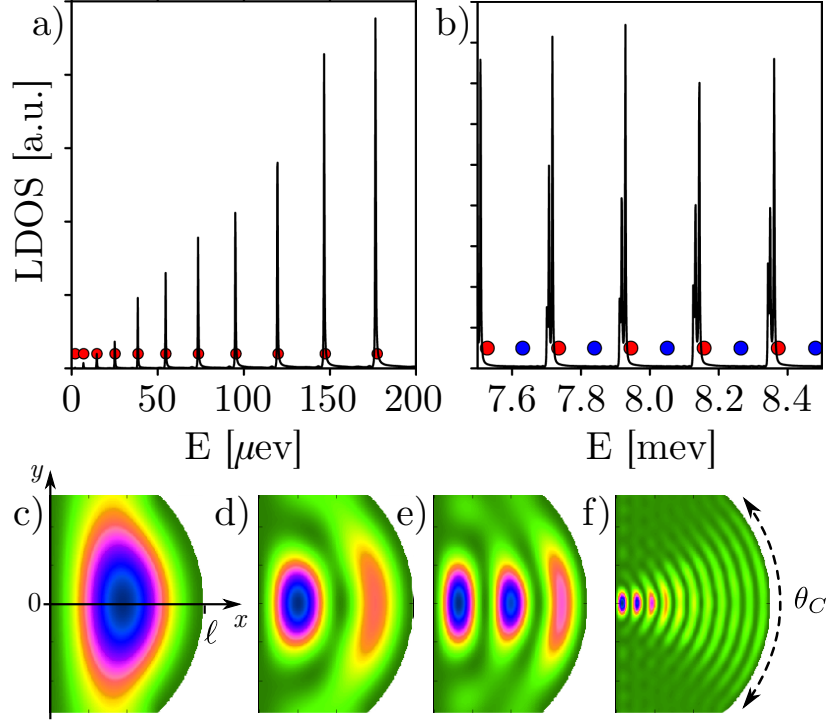


FIG. S3. (a) LDOS calculated via Kwant near $r = 0$ as a function of energy for ranges around (a) low energy, and (b) energy near $\varepsilon_F = 8$ meV. In (a) the peaks match the $n = 1$ Bessel mode energies indicated by the red circles. In (b) the red (blue) dots are the odd (even) l Bessel mode energies. The data corresponds to a grid step size of 2 nm, which is close to numerical convergence. The energy spacing between the LDOS peaks match δ_{cav} between odd l modes (red dots). The agreement with the odd Bessel modes improve as the step size is reduced, but a small discrepancy can be expected due to the real energy shift introduced by the self-energy of the leads. (c)-(f) Full LDOS map for first peaks in panel (a), with energies $\sim 2, 7, 15$, and $180 \mu\text{eV}$.

dependent hybridization functions. The NRG, on the other hand, provides an robust approach to treat strongly correlated many-body systems and is amenable for including non-trivial geometric effects beyond the wide band limit.

Before presenting the details of the calculation of the current, let us address the hybridization function of the experimental system of interest and discuss some of the implications of our findings.

Let us begin by writing the Green's functions in the Zubarev notation, namely,

$$G_{A,B}(\omega) \equiv \langle \langle A; B \rangle \rangle_{\omega} \quad (\text{S6})$$

with the corresponding equations of motion (EOMs):

$$\begin{aligned} \omega \langle \langle A; B \rangle \rangle &= \langle \{A; B\} \rangle + \langle \langle [A, H]; B \rangle \rangle \\ &= \langle \{A; B\} \rangle - \langle \langle A; [B, H] \rangle \rangle \end{aligned} \quad (\text{S7})$$

that have the same form for the retarded, advanced, and time-ordered Green's functions (GFs). These GFs are computed for all combinations of creation and annihilation operators in our model system. (The later correspond to d_{σ} , $c_{\alpha\mathbf{k}\sigma}$, and $a_{j\sigma}$ that are defined in the main text.) In what follows, we shall omit the spin label σ , and indicate the type of Green's function only when necessary.

Using these results, one readily obtains a set of coupled Green's functions for our model Hamiltonian, defined in

paper. These read

$$(\omega - \varepsilon_i)G_{id}(\omega) = \sum_{\mathbf{k}} V_{j\mathbf{k}} G_{R\mathbf{k},d}(\omega) + V_{id}^* G_{dd}(\omega), \quad (\text{S8})$$

$$(\omega - \varepsilon_{\alpha\mathbf{k}})G_{\alpha\mathbf{k},d}(\omega) = V_{\alpha d}^* G_{dd}(\omega) + \delta_{\alpha R} \sum_i V_{iR}^* G_{id}(\omega), \quad (\text{S9})$$

$$(\omega - \varepsilon_i)G_{i,j}(\omega) = \delta_{ij} + V_{id}^* G_{di}(\omega) + \sum_{\mathbf{k}} V_{iR} G_{R\mathbf{k},j}(\omega), \quad (\text{S10})$$

$$(\omega - \varepsilon_{\alpha\mathbf{k}})G_{\alpha\mathbf{k},j}(\omega) = V_{d\alpha}^* G_{dj}(\omega) + \delta_{\alpha R} \sum_i V_{iR}^* G_{ij}(\omega). \quad (\text{S11})$$

We use the indices i and j to label cavity modes and d to denote the quantum dot level. In the main text, we use the standard shorthand notation $G_d \equiv G_{dd}$ for the quantum dot Green's function.

Using the expressions above, we can “close” the EOMs (for $U = 0$) and write the retarded quantum dot Green's function for the fully connected system in the absence of electron-electron interactions as

$$G_d^{(0),r}(\omega) = \frac{1}{\omega - \varepsilon_d - \Sigma_d^{(0),r}(\omega)}, \quad (\text{S12})$$

where the expression for $\Sigma_d^{(0),r}(\omega)$ is given in the main text. We define the energy-dependent effective hybridization function $\Delta(\omega) \equiv -\text{Im} \Sigma_d^{(0),r}(\omega)$.

Illustrative examples of $\Delta(\omega = 0)$ ($\omega = 0$ is the Fermi level) vs ϵ_c , are shown in Fig. S4 for both weak and strong-coupling regimes. The drastically different dependence on ϵ_c in both cases is also reflected in contrasting ω dependence at fixed cavity parameters (not shown), which strongly affects the effective spin fluctuations that set in once interactions are considered. As we will show below, this behavior has important consequences for the zero-bias conductance of the system, among other observables.

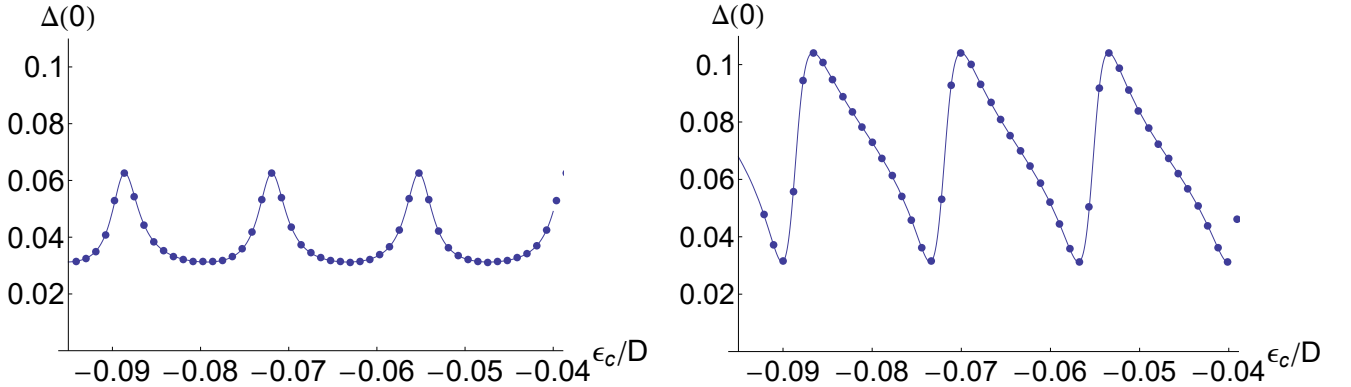


FIG. S4. (color online) Thin line: Effective hybridization function at the Fermi energy $\Delta(\omega=0)$ for weak ($\Omega = 0.001D$, left) and strong ($\Omega = 0.025D$, right) coupling of the QD to the cavity, as function of the cavity gate-voltage ϵ_c/D . Filled circles indicate the ϵ_c/D values points used in Fig. 2 of the main text.

III. DETAILS OF THE NRG CALCULATIONS

The NRG calculations were carried out using an effective single-site Anderson model for a symmetric impurity ($\varepsilon_d = -U/2$) with an hybridization function given by $\Delta(\omega)$. The discretization of the effective band was carried out as discussed in Refs. S4–S6 using a discretization parameter $\Lambda = 2.5$ and z-trick averaging ($N_z = 5$). In the calculations, we explored charge and $SU(2)$ spin symmetries and up to 1000 Q, S states were retained at each NRG iteration.

The spectral density data shown in the paper were obtained using the DM-NRG method.[S7] Additional runs using the CFS approach[S8, S9] were also performed to check convergence of the results.

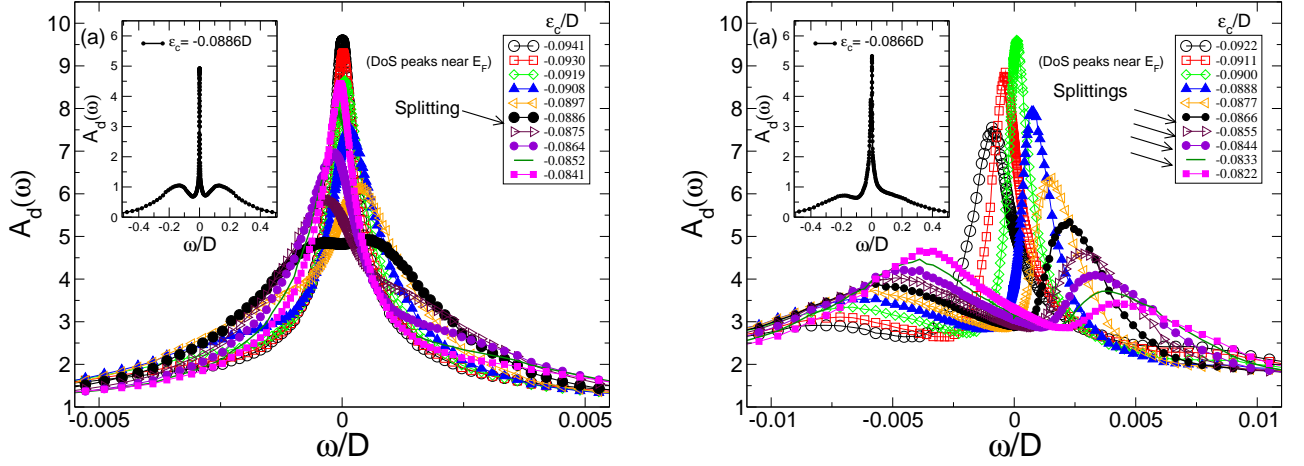


FIG. S5. (color online) NRG spectral functions for (a) $\Omega=0.001D$ and (b) $\Omega=0.025D$ and different values of ϵ_c (same data is shown as a contour plot in Fig. 2 of the main text). Very narrow peaks near $\omega=0$ appear as a result of peak splitting due to the cavity-originated resonances in $\Delta(0)$. The insets show a typical data for ϵ_c values at the resonances of $\Delta(0)$ (see Figs. S4). Notice the broader resonance for $\Omega=0.025D$ [panel (b)] indicating a larger Kondo temperature.

Examples for the results (data in Fig. 2 of the main paper) are presented in Fig. S5. Notice the formation of the Kondo resonance in the insets, with a broader peak for $\Omega=0.025D$ indicating a larger T_K , as discussed in the main text.

IV. CALCULATION OF THE CURRENT THROUGH THE SYSTEM

A. Extension of the Meir-Wingreen formalism

In general, the current flowing from the α contact can be written as

$$J_\alpha = -e \left\langle \frac{d}{dt} N_\alpha \right\rangle \quad (\text{S13})$$

where $N_\alpha = \sum_{\mathbf{k}\sigma} c_{\alpha\mathbf{k}\sigma}^\dagger c_{\alpha\mathbf{k}\sigma}$ counts the number of electrons at lead α . Let us start with the right lead ($\alpha = R$). Using the Heisenberg picture, where $i\hbar\dot{c}_{R\mathbf{k}\sigma} = [c_{R\mathbf{k}\sigma}, H]$, one obtains

$$J_R(t) = -e \sum_{\mathbf{k}\sigma} \left[\sum_i V_{iR} G_{R\mathbf{k}\sigma, i\sigma}^<(t, t) + V_{dR} G_{R\mathbf{k}\sigma, d\sigma}^<(t, t) - \text{H.c.} \right], \quad (\text{S14})$$

where the following Green's functions were introduced,

$$G_{R\mathbf{k}\sigma, i\sigma}^<(t, t') = \frac{i}{\hbar} \langle a_{i\sigma}^\dagger(t') c_{R\mathbf{k}\sigma}(t) \rangle, \quad (\text{S15})$$

$$G_{R\mathbf{k}\sigma, d\sigma}^<(t, t') = \frac{i}{\hbar} \langle c_{d\sigma}^\dagger(t') c_{R\mathbf{k}\sigma}(t) \rangle. \quad (\text{S16})$$

The current J_R is real, since [S10] $G_{ab}^<(t, t) = -[G_{ba}^<(t, t)]^*$.

We are interested in the stationary regime, where J_R does not depend on time. Thus, it is convenient to write Eq. (S14) in the frequency representation,

$$J_R = 2e \text{Re} \left\{ \sum_{\mathbf{k}\sigma} \int \frac{d\omega}{2\pi\hbar} \left[\sum_i V_{iR} G_{R\mathbf{k}\sigma, i\sigma}^<(\omega) + V_{dR} G_{R\mathbf{k}\sigma, d\sigma}^<(\omega) \right] \right\}. \quad (\text{S17})$$

The above equation is the generalization of the two-terminal Meir-Wingreen formula [S11] for our model system, where the right lead ($\alpha = R$) is coupled to both the dot and the cavity; see Fig. 1 of the paper.

In contrast, the left lead ($\alpha = L$) is only coupled to the dot. Consequently, the current J_L is given by the standard expression

$$J_L = 2e \operatorname{Re} \left\{ \sum_{\mathbf{k}\sigma} \int \frac{d\omega}{2\pi\hbar} \left[V_{dL} G_{L\mathbf{k}\sigma, d\sigma}^<(\omega) \right] \right\}. \quad (\text{S18})$$

Next, we use the method of equations of motion (EOM) and the Langreth rules [S12, S13] to express the Green's function $G_{i\sigma, R\mathbf{k}\sigma}^<(\omega)$ in a convenient form.

Using the results of Section II, the contact Green's functions $G_{R\mathbf{k}, d}$ and $G_{R\mathbf{k}, j}$ that appear in Eq. (S17) can be expressed as

$$G_{R\mathbf{k}, d}(\omega) = \frac{V_{dR}^*}{\omega - \varepsilon_{R\mathbf{k}}} G_{dd}(\omega) + \frac{1}{\omega - \varepsilon_{R\mathbf{k}}} \sum_i V_{iR}^* G_{id}(\omega) = g_{R\mathbf{k}}(\omega) V_{dR}^* G_{dd}(\omega) + g_{R\mathbf{k}}(\omega) \sum_i V_{iR}^* G_{id}(\omega) \quad (\text{S19})$$

and

$$G_{R\mathbf{k}, j}(\omega) = \frac{V_{dR}^*}{\omega - \varepsilon_{R\mathbf{k}}} G_{dj}(\omega) + \frac{1}{\omega - \varepsilon_{R\mathbf{k}}} \sum_i V_{iR}^* G_{ij}(\omega) = g_{R\mathbf{k}}(\omega) V_{dR}^* G_{dj}(\omega) + g_{R\mathbf{k}}(\omega) \sum_i V_{iR}^* G_{ij}(\omega), \quad (\text{S20})$$

where $g_{R\mathbf{k}}(\omega)$ is the free Green's function at the terminal R .

Recall that in the simple two-terminal case one has to deal only with $G_{R\mathbf{k}, d} = g_{R\mathbf{k}} V_{dR}^* G_{dd}$. This means that the problem is reduced to the calculation of G_{dd} , see Section VI. Our goal here is similar: we want to eliminate all hybrid (or contact) Green's function and express the current in terms of G_{dd} only.

Let us now solve for G_{jd} . By inserting Eq. (S19) into (S8) we write

$$(\omega - \varepsilon_j) G_{jd}(\omega) = V_{jd}^* G_{dd}(\omega) + \sum_{\mathbf{k}} \frac{V_{jR} V_{dR}^*}{\omega - \varepsilon_{R\mathbf{k}}} G_{dd}(\omega) + \sum_{\mathbf{k}, i} V_{jR} \frac{1}{\omega - \varepsilon_{R\mathbf{k}}} V_{iR}^* G_{id}(\omega). \quad (\text{S21})$$

Hence

$$\sum_i \left[(\omega - \varepsilon_i) \delta_{ij} - \sum_{\mathbf{k}} V_{jR} \frac{1}{\omega - \varepsilon_{R\mathbf{k}}} V_{iR}^* \right] G_{id}(\omega) = \left[V_{jd} + \sum_{\mathbf{k}} V_{jR} \frac{1}{\omega - \varepsilon_{R\mathbf{k}}} V_{dR}^* \right] G_{dd}(\omega) \quad (\text{S22})$$

Next, let us solve for G_{ij} . By inserting Eq. (S20) into (S10) we get

$$(\omega - \varepsilon_i) G_{ij}(\omega) = \delta_{ij} + \sum_{\mathbf{k}} V_{iR} \frac{1}{\omega - \varepsilon_{R\mathbf{k}}} V_{dR}^* G_{dj}(\omega) + \sum_{\mathbf{k}, l} V_{iR} \frac{1}{\omega - \varepsilon_{R\mathbf{k}}} V_{lR}^* G_{lj}(\omega) + V_{id}^* G_{dj}(\omega). \quad (\text{S23})$$

Hence,

$$\sum_l \left[(\omega - \varepsilon_l) \delta_{lj} - \sum_{\mathbf{k}} V_{iR} \frac{1}{\omega - \varepsilon_{R\mathbf{k}}} V_{lR}^* \right] G_{lj}(\omega) = \delta_{ij} + \left[V_{id} + \sum_{\mathbf{k}} V_{iR} \frac{1}{\omega - \varepsilon_{R\mathbf{k}}} V_{dR}^* \right] G_{dj}(\omega). \quad (\text{S24})$$

Before we proceed, let us simplify the notation by introducing the resonance self-energies

$$\Sigma_{\nu\nu'}^\alpha(\omega) = \sum_{\mathbf{k}} V_{\nu\alpha} \frac{1}{\omega - \varepsilon_{\alpha\mathbf{k}}} V_{\nu'\alpha}^* \quad (\text{S25})$$

where $\nu = i, d$. Let us also define

$$\sum_l [(\omega - \varepsilon_l) \delta_{li} - \Sigma_{il}^R(\omega)] G_{lj}^{(0)}(\omega) = \delta_{ij}. \quad (\text{S26})$$

Collecting the results, we obtain

$$G_{id}(\omega) = \sum_j G_{ij}^{(0)}(\omega) [V_{jd} + \Sigma_{jd}^R(\omega)] G_{dd}(\omega) \quad (\text{S27})$$

and

$$G_{ij}(\omega) = G_{ij}^{(0)}(\omega) + \sum_l G_{il}^{(0)}(\omega) [V_{ld} + \Sigma_{ld}^R(\omega)] G_{dj}(\omega). \quad (\text{S28})$$

Note that the integrand in Eq. (S17) contains the Green's functions $G_{i\sigma, R\mathbf{k}\sigma}^<(\omega)$ and $G_{d\sigma, R\mathbf{k}\sigma}^<(\omega)$. Using the Langreth rules [S12] and the Eqs. (S19) and (S20) we write

$$G_{d, R\mathbf{k}}^<(\omega) = G_{dd}^r(\omega) V_{dR} g_{R\mathbf{k}}^<(\omega) + G_{dd}^<(\omega) V_{dR} g_{R\mathbf{k}}^a(\omega) + \sum_i G_{id}^r(\omega) V_{iR} g_{R\mathbf{k}}^<(\omega) + \sum_i G_{id}^<(\omega) V_{iR} g_{R\mathbf{k}}^a(\omega) \quad (\text{S29})$$

and

$$G_{j, R\mathbf{k}}^<(\omega) = G_{jd}^r(\omega) V_{dR} g_{R\mathbf{k}}^<(\omega) + G_{jd}^<(\omega) V_{dR} g_{R\mathbf{k}}^a(\omega) + \sum_i [G_{ji}^r(\omega) V_{iR} g_{R\mathbf{k}}^<(\omega) + G_{ji}^<(\omega) V_{iR} g_{R\mathbf{k}}^a(\omega)] \quad (\text{S30})$$

where the free Green's functions are given by

$$g_{\alpha\mathbf{k}}^{r(a)}(\omega) = \frac{1}{\omega - \varepsilon_{\alpha\mathbf{k}} \pm i0} = \text{PV} \frac{1}{\omega - \varepsilon_{\alpha\mathbf{k}}} \mp i\pi\delta(\omega - \varepsilon_{\alpha\mathbf{k}}) \quad (\text{S31})$$

and $g_{\alpha\mathbf{k}}^<(\omega) = 2\pi i\delta(\omega - \varepsilon_{\alpha\mathbf{k}}) f_{\alpha}(\omega)$.

In the wide band limit we can evaluate the self-energies as

$$\Sigma_{\nu\nu'}^{\alpha, r/a}(\omega) = \mp i\pi V_{\nu\alpha} \rho_{\alpha} V_{\nu'}^* \quad (\text{S32})$$

where ρ_{α} is density of states of the reservoir $\alpha = R, L$. From this expression we can define $\Sigma_{\nu\nu'}^{\alpha, r}(\omega) = -i\pi V_{\nu\alpha} \rho_{\alpha} V_{\nu'}^* \equiv -i\Gamma_{\nu\alpha}/2$, and assuming the couplings real, $\Sigma_{id}^{\alpha, r}(\omega) = -i\pi V_{i\alpha} \rho_{\alpha} V_{d\alpha}^* = -i\sqrt{\Gamma_{iR}\Gamma_{dR}}/2$. Notice that this definition of $\Gamma_{\nu\alpha}$ (more frequent in transport works) carries an extra fact of 2 as compared to the definition commonly used by the strongly-correlated systems community (" $\Gamma = \pi\rho|V|^2$ ").

We now introduce the new self-energies

$$\tilde{\Sigma}_{jd}^{R, a}(\omega) = V_{jd} + i\sqrt{\Gamma_{jR}\Gamma_{dR}}/2, \quad (\text{S33})$$

$$\tilde{\Sigma}_{jd}^{R, r}(\omega) = V_{jd} - i\sqrt{\Gamma_{jR}\Gamma_{dR}}/2, \quad (\text{S34})$$

and

$$\tilde{\Sigma}_{jd}^{R, <}(\omega) = +if_R(\omega)\sqrt{\Gamma_{jR}\Gamma_{dR}}. \quad (\text{S35})$$

Using the Langreth rules[S12] we are able to express G_{id} and G_{ij} , given by Eqs. (S28) and (S27), in terms of free Green's functions (that we know analytically) and of G_{dd} . Combining Eqs. (S27) and (S28) with (S33)- (S35) we can write

$$G_{id}^{r(a)}(\omega) = \sum_j G_{ij}^{(0), r(a)}(\omega) \tilde{\Sigma}_{jd}^{R, r(a)}(\omega) G_{dd}^{r(a)}(\omega), \quad (\text{S36})$$

$$G_{id}^<(\omega) = \sum_j \left[G_{ij}^{(0), r}(\omega) \tilde{\Sigma}_{jd}^{R, r}(\omega) G_{dd}^<(\omega) + G_{ij}^{(0), r}(\omega) \tilde{\Sigma}_{jd}^{R, <}(\omega) G_{dd}^a(\omega) + G_{ij}^{(0), <}(\omega) \tilde{\Sigma}_{jd}^{R, a}(\omega) G_{dd}^a(\omega) \right], \quad (\text{S37})$$

$$G_{di}^<(\omega) = \sum_j \left[G_{dd}^r(\omega) \tilde{\Sigma}_{dj}^{R, r}(\omega) G_{ji}^{(0), <}(\omega) + G_{dd}^r(\omega) \tilde{\Sigma}_{dj}^{R, <}(\omega) G_{ji}^{(0), a}(\omega) + G_{dd}^<(\omega) \tilde{\Sigma}_{dj}^{R, a}(\omega) G_{ji}^{(0), a}(\omega) \right], \quad (\text{S38})$$

and

$$\begin{aligned} G_{ij}^<(\omega) = & G_{ij}^{(0), <}(\omega) + \sum_{l'} \left[G_{il}^{(0), r}(\omega) \tilde{\Sigma}_{ld}^{R, r}(\omega) G_{dd}^r(\omega) \tilde{\Sigma}_{dl'}^{R, r}(\omega) G_{l'j}^{(0), <}(\omega) + G_{il}^{(0), r}(\omega) \tilde{\Sigma}_{ld}^{R, r}(\omega) G_{dd}^r(\omega) \tilde{\Sigma}_{dl'}^{R, <}(\omega) G_{l'j}^{(0), a}(\omega) \right. \\ & + G_{il}^{(0), r}(\omega) \tilde{\Sigma}_{ld}^{R, r}(\omega) G_{dd}^<(\omega) \tilde{\Sigma}_{dl'}^{R, a}(\omega) G_{l'j}^{(0), a}(\omega) + G_{il}^{(0), r}(\omega) \tilde{\Sigma}_{ld}^{R, <}(\omega) G_{dd}^a(\omega) \tilde{\Sigma}_{dl'}^{R, a}(\omega) G_{l'j}^{(0), a}(\omega) \\ & \left. + G_{il}^{(0), <}(\omega) \tilde{\Sigma}_{ld}^{R, a}(\omega) G_{dd}^a(\omega) \tilde{\Sigma}_{dl'}^{R, a}(\omega) G_{l'j}^{(0), a}(\omega) \right]. \end{aligned} \quad (\text{S39})$$

We are now ready to return to Eq. (S17) and calculate the current $J_R \equiv J_R^{(1)} + J_R^{(2)}$, with

$$J_R^{(1)} = 2e \sum_{\mathbf{k}\sigma} \sum_i \text{Re} \int \frac{d\omega}{2\pi\hbar} \left\{ G_{id}^r(\omega) V_{dR} 2\pi i \delta(\omega - \varepsilon_{\mathbf{k}}) f_R(\omega) V_{iR}^* + G_{id}^<(\omega) V_{dR} i\pi \delta(\omega - \varepsilon_{\mathbf{k}}) V_{iR}^* \right. \\ \left. + \sum_j [G_{ij}^r(\omega) V_{jR} 2\pi i \delta(\omega - \varepsilon_{\mathbf{k}}) f_R(\omega) V_{iR}^* + G_{ij}^<(\omega) V_{jR} i\pi \delta(\omega - \varepsilon_{\mathbf{k}}) V_{iR}^*] \right\} \quad (\text{S40})$$

and

$$J_R^{(2)} = 2e \sum_{\mathbf{k}\sigma} \text{Re} \int \frac{d\omega}{2\pi\hbar} \left\{ G_{dd}^r(\omega) V_{dR} 2\pi i \delta(\omega - \varepsilon_{\mathbf{k}}) f_R(\omega) V_{dR}^* + G_{dd}^<(\omega) V_{dR} i\pi \delta(\omega - \varepsilon_{\mathbf{k}}) V_{dR}^* \right. \\ \left. + \sum_i [G_{di}^r(\omega) V_{iR} 2\pi i \delta(\omega - \varepsilon_{\mathbf{k}}) f_R(\omega) V_{dR}^* + G_{di}^<(\omega) V_{iR} i\pi \delta(\omega - \varepsilon_{\mathbf{k}}) V_{dR}^*] \right\}, \quad (\text{S41})$$

where we have used the wide flat band approximation to get rid of the Cauchy principal value contribution.

We now convert the summations over \mathbf{k} into energy integrations, namely

$$\sum_{\mathbf{k}} [\dots] = \int d\varepsilon_{\mathbf{k}} \rho_{\alpha}(\varepsilon_{\mathbf{k}}) [\dots]. \quad (\text{S42})$$

For notational simplicity, let us assume that all coupling matrix elements V are real to write

$$J_R^{(1)} = \frac{e}{\hbar} \sum_{i\sigma} \text{Re} \int \frac{d\omega}{2\pi} \left\{ i\sqrt{\Gamma_{dR}\Gamma_{iR}} [2f_R(\omega)G_{id}^r(\omega) + G_{jd}^<(\omega)] + \sum_j i\sqrt{\Gamma_{jR}\Gamma_{iR}} [2f_R(\omega)G_{ij}^r(\omega) + G_{ij}^<(\omega)] \right\} \\ = \frac{e}{\hbar} \sum_{i\sigma} \int \frac{d\omega}{2\pi} \left\{ \sqrt{\Gamma_{dR}\Gamma_{iR}} [2f_R(\omega)\text{Re}[iG_{id}^r(\omega)] + \text{Re}[iG_{jd}^<(\omega)]] + \sum_j \sqrt{\Gamma_{jR}\Gamma_{iR}} [2f_R(\omega)\text{Re}[iG_{ij}^r(\omega)] + \text{Re}[iG_{ij}^<(\omega)]] \right\} \quad (\text{S43})$$

and

$$J_R^{(2)} = \frac{e}{\hbar} \sum_{\sigma} \text{Re} \int \frac{d\omega}{2\pi} \left\{ i\Gamma_{dR} [2f_R(\omega)G_{dd}^r(\omega) + G_{dd}^<(\omega)] + \sum_j i\sqrt{\Gamma_{dR}\Gamma_{jR}} [2f_R(\omega)G_{dj}^r(\omega) + G_{dj}^<(\omega)] \right\} \\ = \frac{e}{\hbar} \sum_{\sigma} \int \frac{d\omega}{2\pi} \left\{ \Gamma_{dR} [2f_R(\omega)\text{Re}[iG_{dd}^r(\omega)] + \text{Re}[iG_{dd}^<(\omega)]] + \sum_j \sqrt{\Gamma_{dR}\Gamma_{jR}} [2f_R(\omega)\text{Re}[iG_{dj}^r(\omega)] + \text{Re}[iG_{dj}^<(\omega)]] \right\}. \quad (\text{S44})$$

We recall that $[G_{a,b}^<(\omega)]^* = -G_{b,a}^<(\omega)$. Therefore $G_{dd}^<(\omega)$ is pure imaginary. For the non-diagonal terms we use $\text{Re}(ic) = i(c - c^*)/2$ to write

Therefore,

$$\text{Re}[iG_{a,b}^<(\omega)] = \frac{i}{2} [G_{a,b}^<(\omega) - [G_{a,b}^<(\omega)]^*] = \frac{i}{2} [G_{a,b}^<(\omega) + G_{b,a}^<(\omega)]. \quad (\text{S45})$$

$$J_R^{(1)} = \frac{ie}{\hbar} \sum_{i\sigma} \int d\omega \sqrt{\Gamma_{iR}} \left\{ \sqrt{\Gamma_{dR}} \left[f_R(\omega) [G_{id}^r(\omega) - G_{id}^a(\omega)] + \frac{1}{2} (G_{id}^<(\omega) + G_{id}^>(\omega)) \right] \right. \\ \left. + \sum_j \sqrt{\Gamma_{jR}} \left[f_R(\omega) [G_{ij}^r(\omega) - G_{ij}^a(\omega)] + \frac{1}{2} (G_{ij}^<(\omega) + G_{ij}^>(\omega)) \right] \right\} \quad (\text{S46})$$

and

$$J_R^{(2)} = \frac{ie}{h} \sum_{\sigma} \int d\omega \left\{ \Gamma_{dR} [f_R(\omega) [G_{dd}^r(\omega) - G_{dd}^a(\omega)] + G_{dd}^<(\omega)] \right. \\ \left. + \sum_j \sqrt{\Gamma_{jR} \Gamma_{dR}} \left[f_R(\omega) [G_{dj}^r(\omega) - G_{dj}^a(\omega)] + \frac{1}{2} (G_{di}^<(\omega) + G_{id}^<(\omega)) \right] \right\} \quad (\text{S47})$$

and finally

$$J_R = \frac{ie}{h} \sum_{\sigma} \int d\omega \left\{ \Gamma_{dR} [f_R(\omega) [G_{dd}^r(\omega) - G_{dd}^a(\omega)] + G_{dd}^<(\omega)] \right. \\ \left. + \sqrt{\Gamma_{dR}} \sum_j \sqrt{\Gamma_{jR}} \left[f_R(\omega) [G_{dj}^r(\omega) + G_{jd}^r(\omega) - G_{dj}^a(\omega) - G_{jd}^a(\omega)] + G_{dj}^<(\omega) + G_{jd}^<(\omega)] \right] \right. \\ \left. + \sum_{ij} \sqrt{\Gamma_{iR} \Gamma_{jR}} \left[f_R(\omega) [G_{ij}^r(\omega) - G_{ij}^a(\omega)] + \frac{1}{2} (G_{ij}^<(\omega) + G_{ji}^<(\omega)) \right] \right\}. \quad (\text{S48})$$

Using $G^a(\omega) = [G^r(\omega)]^\dagger$ one could simplify somewhat the second line of Eq. (S48) to obtain

$$J_R = \frac{ie}{h} \sum_{\sigma} \int d\omega \left\{ \Gamma_{dR} [f_R(\omega) [G_{dd}^r(\omega) - G_{dd}^a(\omega)] + G_{dd}^<(\omega)] \right. \\ \left. + 2\sqrt{\Gamma_{dR}} \sum_j \sqrt{\Gamma_{jR}} \left[f_R(\omega) [G_{jd}^r(\omega) - G_{jd}^a(\omega)] + \frac{1}{2} (G_{jd}^<(\omega) + G_{dj}^<(\omega)) \right] \right. \\ \left. + \sum_{ij} \sqrt{\Gamma_{iR} \Gamma_{jR}} \left[f_R(\omega) [G_{ij}^r(\omega) - G_{ij}^a(\omega)] + \frac{1}{2} (G_{ij}^<(\omega) + G_{ji}^<(\omega)) \right] \right\}. \quad (\text{S49})$$

Inserting the expressions for the lesser Green's function we obtain

$$J_R = \frac{ie}{h} \sum_{\sigma} \int d\omega \left\{ \Gamma_{dR} [f_R(\omega) [G_{dd}^r(\omega) - G_{dd}^a(\omega)] + G_{dd}^<(\omega)] \right. \\ \left. + 2\sqrt{\Gamma_{dR}} \sum_j \sqrt{\Gamma_{jR}} \left\{ f_R(\omega) [G_{jd}^r(\omega) - G_{jd}^a(\omega)] + \frac{1}{2} \sum_l [G_{jl}^{(0),r}(\omega) \tilde{\Sigma}_{ld}^{R,r}(\omega) + G_{lj}^{(0),a}(\omega) \tilde{\Sigma}_{dl}^{R,a}(\omega)] G_{dd}^<(\omega) \right. \right. \\ \left. + [G_{lj}^{(0),a}(\omega) \tilde{\Sigma}_{dl}^{R,<}(\omega) + G_{lj}^{(0),<}(\omega) \tilde{\Sigma}_{dl}^{R,r}(\omega)] G_{dd}^r(\omega) + [G_{jl}^{(0),r}(\omega) \tilde{\Sigma}_{ld}^{R,<}(\omega) + G_{jl}^{(0),<}(\omega) \tilde{\Sigma}_{ld}^{R,a}(\omega)] G_{dd}^a(\omega) \right\} \\ \left. + \sum_{ij} \sqrt{\Gamma_{iR} \Gamma_{jR}} \left\{ f_R(\omega) [G_{ij}^r(\omega) - G_{ij}^a(\omega)] + \frac{1}{2} (G_{ij}^{(0),<}(\omega) + G_{ji}^{(0),<}(\omega)) \right. \right. \\ \left. + \frac{1}{2} \sum_{l'l'} (G_{il}^{(0),r}(\omega) \tilde{\Sigma}_{ld}^{R,r}(\omega) \tilde{\Sigma}_{dl'}^{R,a}(\omega) G_{l'j}^{(0),a}(\omega) + G_{jl'}^{(0),r}(\omega) \tilde{\Sigma}_{l'd}^{R,r}(\omega) \tilde{\Sigma}_{dl}^{R,a}(\omega) G_{li}^{(0),a}(\omega)) G_{dd}^<(\omega) \right. \\ \left. + [G_{il}^{(0),r} \tilde{\Sigma}_{ld}^{R,r} (\tilde{\Sigma}_{dl'}^{R,r} G_{l'j}^{(0),<} + \tilde{\Sigma}_{dl'}^{R,<} G_{l'j}^{(0),a}) + G_{jl'}^{(0),r} \tilde{\Sigma}_{l'd}^{R,r} (\tilde{\Sigma}_{dl}^{R,r} G_{li}^{(0),<} + \tilde{\Sigma}_{dl}^{R,<} G_{li}^{(0),a})] G_{dd}^r(\omega) \right. \\ \left. + [(G_{il}^{(0),r} \tilde{\Sigma}_{ld}^{R,<} + G_{il}^{(0),<} \tilde{\Sigma}_{ld}^{R,a}) \tilde{\Sigma}_{dl'}^{R,a} G_{l'j}^{(0),a} + (G_{jl'}^{(0),r} \tilde{\Sigma}_{l'd}^{R,<} + G_{jl'}^{(0),<} \tilde{\Sigma}_{l'd}^{R,a}) \tilde{\Sigma}_{dl}^{R,a} G_{li}^{(0),a}] G_{dd}^a(\omega) \right\} \right\}. \quad (\text{S50})$$

In the above we need to know that

$$G_{ij}^{(0),r}(\omega) = [\omega - H_{\text{cavity}} - \Sigma^{R,r}(\omega)]_{ij}^{-1}, \quad (\text{S51})$$

$$G_{ij}^{(0),a}(\omega) = [\omega - H_{\text{cavity}} - \Sigma^{R,a}(\omega)]_{ij}^{-1}, \quad (\text{S52})$$

$$G_{ij}^{(0),<}(\omega) = \sum_l G_{il}^{(0),r}(\omega) \Sigma_{ll'}^{R,<}(\omega) G_{l'j}^{(0),a}(\omega), \quad (\text{S53})$$

This lengthy expression reduces to the standard expression for the current found in Meir-Wingreen when one considers the simple case without cavity, that is, $\Gamma_{iR} = 0$.

corresponds to the cavity Green's function in the absence

of the dot.

B. Expressions for the current

We now write the results of Eq. (S50) for the simplified model. First note that by assuming that the coupling of all the cavity levels with the right reservoir are equal, i.e., $V_{iR} = V_{cR}$ for all i in the cavity. Then $\Sigma_{ij}^R(\omega) = -i\Gamma_{cR}/2$, $\Sigma_{id}^R(\omega) = -i\sqrt{\Gamma_{dR}\Gamma_{cR}}/2$. The lesser GF can be written as $\Sigma_{ij}^{R,<}(\omega) = if_R(\omega)\Gamma_{cR}$ using the fact that $\sum_{\mathbf{k}} g_{\mathbf{k},R}^<(\omega) = 2i\pi\rho_R f_R(\omega)$. Assuming also $V_{di} = \Omega$ for all dot-level coupling matrix elements, the self-energies defined in Eqs. (S33) to (S35) can also be simplified,

$$\tilde{\Sigma}_{jd}^{R,(a,r)}(\omega) = \Omega \pm i\sqrt{\Gamma_{dR}\Gamma_{cR}}/2 \quad (\text{S54})$$

$$\tilde{\Sigma}_{jd}^{R,<}(\omega) = +if_R(\omega)\sqrt{\Gamma_{dR}\Gamma_{cR}}. \quad (\text{S55})$$

We can use the method of equations of motion (EOM) to write J_R and J_R in terms of the Green's function for the dot. Using the Eqs. (S54) into Eq. (S26) we write

$$\sum_{ij} G_{ij}^{(0),r}(\omega) = \tilde{S}(\omega), \quad (\text{S56})$$

with $\tilde{S}(\omega) = S(\omega)(1+iS(\omega)\Gamma_{cR}/2)^{-1}$, where $S = \sum_i(\omega - \varepsilon_i)^{-1}$. The lesser GF becomes

$$\sum_{ij} G_{ij}^{(0),<}(\omega) = if_R(\omega)\Gamma_{cR} \left| \tilde{S}(\omega) \right|^2. \quad (\text{S57})$$

From there, we can write the other Green's functions we are going to need in terms of dots GFs:

$$\sum_i G_{id}^r(\omega) = \tilde{S}(\omega) \left(\Omega - i\sqrt{\Gamma_{cR}\Gamma_{dR}}/2 \right) G_{dd}^r(\omega), \quad (\text{S58})$$

$$\sum_{ij} G_{ij}^r(\omega) = \tilde{S}(\omega) \left[1 + \tilde{S}(\omega) \left(\Omega - i\sqrt{\Gamma_{cR}\Gamma_{dR}}/2 \right)^2 G_{dd}^r(\omega) \right]. \quad (\text{S59})$$

We are now in a position of re-writing Eq. (S50) for this simplified model. Lets start with by writing it in terms of the GFs defined above (sums included). Using Eqs. (S32), (S54), and (S55), the Eq. (S50) becomes

$$\begin{aligned} J_R = & \frac{ie}{h} \sum_{\sigma} \int d\omega \left\{ \Gamma_{dR} \left[f_R(\omega) (G_{dd}^r - G_{dd}^a) + G_{dd}^{<} \right] + 2\sqrt{\Gamma_{dR}\Gamma_{cR}} \left\{ f_R(\omega) \left[\sum_j G_{jd}^r - \sum_j G_{jd}^a \right] \right. \right. \\ & + \frac{1}{2} \left[\left(\sum_{jl} G_{jl}^{(0),r} \right) \left(\Omega - \frac{i}{2}\sqrt{\Gamma_{dR}\Gamma_{cR}} \right) + \left(\sum_{jl} G_{jl}^{(0),a} \right) \left(\Omega + \frac{i}{2}\sqrt{\Gamma_{dR}\Gamma_{cR}} \right) \right] G_{dd}^{<} \\ & + \frac{1}{2} \left[\left(\sum_{jl} G_{lj}^{(0),a} \right) if_R(\omega)\sqrt{\Gamma_{dR}\Gamma_{cR}} + \left(\sum_{jl} G_{lj}^{(0),<} \right) \left(\Omega - \frac{i}{2}\sqrt{\Gamma_{dR}\Gamma_{cR}} \right) \right] G_{dd}^r \\ & + \frac{1}{2} \left[\left(\sum_{jl} G_{jl}^{(0),r} \right) if_R(\omega)\sqrt{\Gamma_{dR}\Gamma_{cR}} + \left(\sum_{jl} G_{jl}^{(0),<} \right) \left(\Omega + \frac{i}{2}\sqrt{\Gamma_{dR}\Gamma_{cR}} \right) \right] G_{dd}^a \left. \right\} \\ & + \Gamma_{cR} \left\{ f_R(\omega) \left(\sum_{ij} G_{ij}^r - \sum_{ij} G_{ij}^a \right) + \sum_{ij} G_{ij}^{(0),<} + \left| \sum_{il} G_{il}^{(0),r} \right|^2 \left(\Omega^2 + \frac{\Gamma_{dR}\Gamma_{cR}}{4} \right) G_{dd}^{<} \right. \\ & + \left(\sum_{il} G_{il}^{(0),r} \right) \left(\Omega - \frac{i}{2}\sqrt{\Gamma_{dR}\Gamma_{cR}} \right) \left[\left(\Omega - \frac{i}{2}\sqrt{\Gamma_{dR}\Gamma_{cR}} \right) \sum_{l'j} G_{l'j}^{(0),<} + if_R(\omega)\sqrt{\Gamma_{dR}\Gamma_{cR}} \sum_{l'j} G_{l'j}^{(0),a} \right] G_{dd}^r \\ & + \left. \left(\sum_{l'j} G_{l'j}^{(0),a} \right) \left(\Omega + \frac{i}{2}\sqrt{\Gamma_{dR}\Gamma_{cR}} \right) \left[\left(\Omega + \frac{i}{2}\sqrt{\Gamma_{dR}\Gamma_{cR}} \right) \sum_{il} G_{il}^{(0),<} + if_R(\omega)\sqrt{\Gamma_{dR}\Gamma_{cR}} \sum_{il} G_{il}^{(0),r} \right] G_{dd}^a \right\} \right\}. \quad (\text{S60}) \end{aligned}$$

We now substitute Eqs. (S56)–(S59) into Eq. (S60) and collect the terms in G_{dd}^r , G_{dd}^r and $G_{dd}^{<}$. Using the limit $\lim_{\eta \rightarrow 0} S(\omega + i\eta)$ (i.e., taking the analytic continuation of $S(\omega)$ to the real axis), and after some long but straight-

forward algebra, we obtain J_R in a nice, compact form:

$$J_R = J_R^{(0)} + \frac{ie}{h} \sum_{\sigma} \int d\omega \Gamma_R(\omega) \left\{ f_R(\omega) [G_{dd}^r(\omega) - G_{dd}^a(\omega)] + G_{dd}^{<}(\omega) \right\}$$

In the equation above, $J_R^{(0)}$ is a background contribution coming from the terms in Eq. (S60) that do not involve dot's Green's functions:

$$J_R^{(0)} = \frac{ie}{h} \sum_{\sigma} \int d\omega \Gamma_{cR} \sum_{ij} \left\{ f_R(\omega) \left[G_{ij}^{(0),r}(\omega) - G_{ij}^{(0),a}(\omega) \right] + G_{ij}^{(0),<}(\omega) \right\}. \quad (S62)$$

In fact, as we will show below, $J_R^{(0)}$ vanish, explicitly, for $\eta \rightarrow 0$. The effective coupling $\Gamma_R(\omega)$ is a *real* algebraic function of the parameters, given by:

$$\Gamma_R(\omega) = \Gamma_{dR} + \Gamma_{cR} \left| \tilde{S}(\omega) \right|^2 \left(\Omega^2 + \frac{\Gamma_{cR}\Gamma_{dR}}{4} \right) + \sqrt{\Gamma_{dR}\Gamma_{cR}} \left[\tilde{S}(\omega) \left(\Omega - \frac{\Gamma_{cR}\Gamma_{dR}}{2} \right) + \text{H.c.} \right] \left[\tilde{S}(\omega) \left(\tilde{\Omega}^* G_{dd}^r - (\tilde{S})^* \tilde{\Omega} G_{dd}^a \right) \right]. \quad (S63)$$

The current from the left lead is simple because $\Gamma_{iL} = 0$, so we have for J_L ,

$$J_L = \frac{ie}{h} \sum_{\sigma} \int d\omega \Gamma_{dL} \left\{ f_L(\omega) [G_{dd}^r(\omega) - G_{dd}^a(\omega)] + G_{dd}^{<}(\omega) \right\}. \quad (S64)$$

V. FLUCTUATION-DISSIPATION THEOREM

An important consistency check for the expressions given in the previous section is the applicability of the fluctuation-dissipation theorem (FDT). For instance, the expression for J_R in Eq. (S61) vanishes in equilibrium, when the fluctuation-dissipation theorem (FDT) applies.

Just a reminder: the FDT states that, for a system in thermal equilibrium with a reservoir described by a Fermi distribution $f_R(\omega)$, the lesser Green's function is proportional to the spectral density:

$$G_{\nu}^{<}(\omega) = 2\pi i f_R(\omega) A_{\nu}(\omega), \quad (S65)$$

where $A_{\nu}(\omega) = (-1/\pi) \text{Im } G_{\nu}^r(\omega)$.

We can put the FDT in terms of retarded and advanced Green's functions. Using $G_{\nu}^a(\omega) = (G_{\nu}^r(\omega))^*$, the FDT implies:

$$G_{\nu}^{<}(\omega) = -f_R(\omega) [G_{\nu}^r(\omega) - G_{\nu}^a(\omega)]. \quad (S66)$$

This is important as a consistency check for the current calculations. Applying Eq. (S66), the current to/from a single lead should vanish (which is the correct result in equilibrium). This can be readily verified, for instance, for $J_R^{(0)}$ defined in Eq. (S62) and for J_L [Eq. (S64)].

In fact, this consistency check can be applied to each of the three terms in Eq. (S49) by verifying that the FDT is satisfied for each of the Green's functions involved. Note that the first term in in Eq. (S49) involves diagonal (dot) GFs and is clearly consistent with the FDT: it vanishes if $G_{dd}^{<}(\omega) = -f_R(\omega) [G_{dd}^r(\omega) - G_{dd}^a(\omega)]$.

The second term involves non-diagonal Greens functions. We can then explicitly show that:

$$\frac{1}{2} \sum_j G_{jd}^{<} + G_{dj}^{<} = -f_R(\omega) \left[\sum_j G_{jd}^r - G_{jd}^a \right]. \quad (S67)$$

The right-hand side of the above expression can be easily calculated using Eq. (S58). Using the short-hand notation:

$$\tilde{S} \equiv \frac{S(\omega)}{1 + iS(\omega)\Gamma_{cR}/2} \quad (S68)$$

$$\tilde{\Omega} \equiv \Omega + i\sqrt{\Gamma_{cR}\Gamma_{dR}}/2, \quad (S69)$$

we have

$$\left[\tilde{S}(\omega) \left(\Omega - \frac{\Gamma_{cR}\Gamma_{dR}}{2} \right) + \text{H.c.} \right] f_R(\omega) \left[\tilde{S}(\omega) \left(\tilde{\Omega}^* G_{dd}^r - (\tilde{S})^* \tilde{\Omega} G_{dd}^a \right) \right]. \quad (S70)$$

Thus, the left-hand side can be calculated with the help of Eqs. (S36) and (S38) and from Eqs. (S54) to (S56), giving:

$$\sum_j G_{jd}^{<} + G_{dj}^{<} = \left(\tilde{S}\tilde{\Omega}^* + \tilde{S}^* \tilde{\Omega} \right) G_{dd}^{<} + i f_R(\omega) \left[\left(\Gamma_{cR} |\tilde{S}|^2 \tilde{\Omega}^* + \sqrt{\Gamma_{cR}\Gamma_{dR}} \right) \right]. \quad (S71)$$

Now, using $G_{dd}^{<}(\omega) = -f_R(\omega) [G_{dd}^r(\omega) - G_{dd}^a(\omega)]$, Eq. (S71) reduces to Eq. (S70). In order to show that, we take the limit $S(\omega) = \lim_{\eta \rightarrow 0} S(\omega + i\eta)$ and then use the following properties:

$$(\tilde{S})^* = \tilde{S} + i\Gamma_{cR} |\tilde{S}|^2 \quad (S72)$$

$$\tilde{\Omega} = (\tilde{\Omega})^* + i\sqrt{\Gamma_{cR}\Gamma_{dR}}. \quad (S73)$$

A similar calculation can be done to show that the third term in Eq. (S49) also satisfies the FDT.

VI. MEIR-WINGREEN-LIKE ELIMINATION OF $G^{<}$

Let us consider the current formula for a single-resonance QD [S11]

$$J_{R(L)} \equiv \int d\omega I_{R(L)}(\omega), \quad (S74)$$

$$I_{R(L)}(\omega) = \frac{ie}{h} \Gamma_{L(R)}(\omega) \left\{ G^{<}(\omega) + f_{L(R)}(\omega) [G^r(\omega) - G^a(\omega)] \right\}. \quad (S75)$$

In the steady state, charge conservation implies that $J_L = -J_R$, hence

$$J_L = \frac{J_L - J_R}{2} \quad (S76)$$

or, in general $J_L = xJ_L - (1-x)J_R$, where x is arbitrary.

We stress that $J_L = -J_R$ is the same as

$$\int d\omega I_L(\omega) = - \int d\omega I_R(\omega), \quad (S77)$$

which *does not* mean that $I_L(\omega) = -I_R(\omega)$ for a given energy ε .

Let us restrict ourselves to the linear response regime and write

$$G^<(\omega) = G_{\text{eq}}^<(\omega) + \frac{\partial G^<}{\partial \mu} \Delta\mu + O(\Delta\mu^2) \quad (\text{S78})$$

$$f_{L(R)}(\omega) = f_0(\omega) \pm \frac{1}{2} \frac{\partial f_0}{\partial \mu} \Delta\mu + O(\Delta\mu^2). \quad (\text{S79})$$

We recall that the fluctuation-dissipation theorem gives

$$G_{\text{eq}}^<(\omega) = -f_0(\omega) [G^r(\omega) - G^a(\omega)],$$

allowing us to write the current $J_{L(R)}$, Eq. (S74), as

$$J_{L(R)} = \frac{ie}{h} \Delta\mu \int d\omega \Gamma_{L(R)}(\omega) \left\{ \frac{\partial G^<}{\partial \mu} \mp \frac{1}{2} \frac{\partial f_0}{\partial \omega} [G^r(\omega) - G^a(\omega)] \right\}, \quad (\text{S80})$$

where \mp refer to the sign of chemical potential offset of L and R terminals with respect to the Fermi energy. Affleck and collaborators [S14] claim that $\partial G^< / \partial \mu$ is expected to have the form $(-\partial f_0 / \partial \omega) \Pi(\omega)$, where (in general) $\Pi(\omega)$ has a smooth energy dependence on the scale of kT . For now, we assume this is true.

Let us assume that $\Gamma_{L(R)}(\omega)$ varies slowly with ε over energies scales of the order of kT , which is a condition met in almost all situations of interest. In this scenario it is safe to approximate

$$J_{L(R)} \approx \frac{ie}{h} \Delta\mu \Gamma_{L(R)}(\varepsilon_F) \int d\omega \left\{ \frac{\partial G^<}{\partial \mu} \pm \frac{1}{2} \left(-\frac{\partial f_0}{\partial \omega} \right) [G^r(\omega) - G^a(\omega)] \right\} \quad (\text{S81})$$

We now use the general relation $J_L = xJ_L - (1-x)J_R$ to write

$$J_L \approx \frac{ie}{h} \Delta\mu \left[x \Gamma_L(\varepsilon_F) \int d\omega \left\{ \frac{\partial G^<}{\partial \mu} + \frac{1}{2} \left(-\frac{\partial f_0}{\partial \omega} \right) [G^r(\omega) - G^a(\omega)] \right\} - (1-x) \Gamma_R(\varepsilon_F) \int d\omega \left\{ \frac{\partial G^<}{\partial \mu} - \frac{1}{2} \left(-\frac{\partial f_0}{\partial \omega} \right) [G^r(\omega) - G^a(\omega)] \right\} \right]. \quad (\text{S82})$$

To eliminate the $G^<$ term one needs $x\Gamma_L - (1-x)\Gamma_R = 0$, yielding $x = \Gamma_R / (\Gamma_L + \Gamma_R)$. Hence

$$J_L \approx \frac{ie}{h} \Delta\mu \frac{\Gamma_L(\varepsilon_F) \Gamma_R(\varepsilon_F)}{\Gamma_L(\varepsilon_F) + \Gamma_R(\varepsilon_F)} \times \int d\omega \left(-\frac{\partial f_0}{\partial \omega} \right) [G^r(\omega) - G^a(\omega)]. \quad (\text{S83})$$

This expression is the same as the one obtained by Meir and Wingreen [S11] using the proportional coupling trick, namely, by assuming that $\Gamma_L(\omega) = \lambda \Gamma_R(\omega)$, where λ does not depend on energy.

From the expression for the current [Eq. (S83)] we can readily derive the corresponding expression for the conductance through the system:

$$G = \frac{2e^2}{h} \frac{\Gamma_{dL} \Gamma_R(\varepsilon_F)}{\Gamma_{dL} + \Gamma_R(\varepsilon_F)} \int d\omega \left(-\frac{\partial f_0}{\partial \omega} \right) A_d(\omega), \quad (\text{S84})$$

where f_0 written in terms of the dot spectral density $A_d(\varepsilon, T) = (-1/\pi) \text{Im } G_{dd}^r(\omega)$ at temperature T that can be calculated with NRG.

-
- [S1] C. Rössler, D. Oehri, O. Zilberberg, G. Blatter, M. Karalic, J. Pijnenburg, A. Hofmann, T. Ihn, K. Ensslin, C. Reichl, and W. Wegscheider, *Phys. Rev. Lett.* **115**, 166603 (2015).
- [S2] M. Abramowitz and I. Stegun, *Handbook of Mathematical Functions: With Formulas, Graphs, and Mathematical Tables*, Applied mathematics series (Dover Publications, 1964).
- [S3] C. W. Groth, M. Wimmer, A. R. Akhmerov, and X. Waintal, *New J. Phys.* **16**, 063065 (2014).
- [S4] C. Gonzalez-Buxton and K. Ingersent, *Phys. Rev. B* **57**,

- 14254 (1998).
- [S5] L. G. G. V. Dias da Silva, K. Ingersent, N. Sandler, and S. Ulloa, *Phys. Rev. B* **78**, 153304 (2008).
- [S6] L. G. G. V. Dias da Silva, N. P. Sandler, K. Ingersent, and S. E. Ulloa, *Phys. Rev. Lett.* **97**, 096603 (2006).
- [S7] W. Hofstetter, *Phys. Rev. Lett.* **85**, 1508 (2000).
- [S8] R. Peters, T. Pruschke, and F. B. Anders, *Phys. Rev. B* **74**, 245114 (2006).
- [S9] A. Weichselbaum and J. von Delft, *Phys. Rev. Lett.* **99**, 076402 (2007).
- [S10] H. Haug and A.-P. Jauho, *Quantum Kinetics in Trans-*

port and Optics of Semiconductors (Springer, New York, 1996).

[S11] Y. Meir and N. S. Wingreen, [Phys. Rev. Lett. **68**, 2512 \(1992\)](#).

[S12] The Langreth rules [\[S13\]](#) we have employed here can be

written as

$$C^r = A^r B^r \Rightarrow C^< = A^r B^< + A^< B^a$$

$$D^r = A^r B^r C^r \Rightarrow D^< = A^r B^r C^< + A^r B^< C^a + A^< B^a C^a,$$

where A , B and C are matrices.

[S13] D. C. Langreth, *Linear and Nonlinear Electron Transport in Solids*, edited by J. T. Devreese and V. E. van Doren (Plenum Press, New York and London, 1976).

[S14] Y. Komijani, R. Yoshii, and I. Affleck, [Phys. Rev. B **88**, 245104 \(2013\)](#).